remote sensing

MDPI

Technical Note

Study of the Tidal Variations in the Ionosphere and the MLT Region over Mohe and Beijing During Six Intense Geomagnetic Storms from 2016 to 2021

Jiarong Ma [1,2], Zheng Ma [1,2,*], Jiaxin Bao [1,2], Jiahui Luo [1,2], Junfeng Yang [2] and Dan Liu [2]

[1] Electronic Information School, Wuhan University, Wuhan 430072, China; majiarong@whu.edu.cn (J.M.); baojiaxin@whu.edu.cn (J.B.); luojiahui@whu.edu.cn (J.L.)
[2] State Key Laboratory of Space Weather, National Space Science Center, Chinese Academy of Sciences, Beijing 100190, China; yangjunfeng@nssc.ac.cn (J.Y.); liudan@nssc.ac.cn (D.L.)
* Correspondence: mazheng@whu.edu.cn

Abstract: Geomagnetic storms can cause large variations in the ionosphere, but their impacts on the mesosphere and lower thermosphere (MLT) are not well understood. Based on the Total Electron Content (TEC) data and the meteor neutral winds data over Mohe (53.5°N, 122.3°E) and Beijing (40.3°N, 116.2°E), we analyze the tidal variations during six intense geomagnetic storms from 2016 to 2021. According to the six intense geomagnetic storms, we found that intense geomagnetic storms can lead to diurnal and semidiurnal tidal enhancements in TEC, while their influences on tidal variations in the MLT region are not always captured. Responses of tidal enhancement in the MLT region to the intense geomagnetic storms are more obvious at a lower latitude at Beijing, but the tidal amplitude changes are not proportional to the Dst indices. Some semidiurnal tides are significantly enhanced prior to the onset of geomagnetic storms, which needs to be statistically investigated in the future based on additional observations.

Keywords: semidiurnal tide; geomagnetic storm; mesosphere and lower thermosphere; TEC

Citation: Ma, J.; Ma, Z.; Bao, J.; Luo, J.; Yang, J.; Liu, D. Study of the Tidal Variations in the Ionosphere and the MLT Region over Mohe and Beijing During Six Intense Geomagnetic Storms from 2016 to 2021. *Remote Sens.* **2024**, *16*, 3947. https://doi.org/10.3390/rs16213947

Academic Editor: Silas Michaelides

Received: 25 September 2024
Revised: 18 October 2024
Accepted: 22 October 2024
Published: 23 October 2024

1. Introduction

Geomagnetic disturbances can have substantial effects on the ionosphere and thermosphere, leading to notable variations in total electron content (TEC), thermospheric compositions, temperature, and neutral winds. During geomagnetic storms, ionospheric TEC can either increase or decrease compared to normal conditions, known as positive or negative storms, respectively [1–8]. Typically, TEC experiences a significant increase during the early phase of a geomagnetic storm. Subsequently, as the storm progresses, it gradually decreases below normal levels before slowly returning to its pre-storm state. Ionospheric disturbances during geomagnetic storms are usually attributed to changes in the thermosphere, including variations in neutral winds and composition that affect ionization rates [6,9]. However, the simultaneous detection of compositions in the ionosphere and thermosphere usually requires strong equipment, such as incoherent scatter radars or satellite missions [10–17]. Consequently, the theoretical variations in temperature and neutral winds during geomagnetic storms are mostly obtained through numerical simulations [18–21]. Previous studies based on the thermosphere-ionosphere-mesosphere-electrodynamics general circulation model (TIMEGCM) indicated that adiabatic heating/cooling and vertical heat advection during geomagnetic storms can influence temperatures in the MLT region at middle latitudes via vertical wind changes [18,19,21]. Nevertheless, the impact of geomagnetic storms on the atmosphere can be both positive and negative, which poses challenges in statistical studies.

Previous studies have also focused on the tidal variations in the ionosphere and thermosphere during geomagnetic storms. Responses of diurnal and semidiurnal migrating

tides in TEC to geomagnetic storms are observed within the 20°S–20°N latitude band [22]. At middle (near ±40°) and high latitudes (near ±60°), the diurnal migrating tide was found to be dominant in the ionospheric anomalies during geomagnetic storms [23]. For tidal waves in neutral winds, Wand (1983) found that during disturbed geomagnetic conditions, semidiurnal tidal amplitudes of the wind are reduced by 20 to 50% at 105 km and 115 km [24]. Manson and Meek (1991) also found a decrease in the amplitudes of diurnal and semidiurnal tides during high geomagnetic activities [25]. Singer et al. (1994) discovered a slightly reduced semidiurnal tidal amplitude in the MLT region at middle latitudes during geomagnetic storms [26]. Zhang et al. (2003) found different responses of the dayside and the nightside MLT winds to the April 2002 geomagnetic storm [27]. Balan et al. (2004) investigated the prevailing wind and tidal features in the MLT region at northern middle latitudes during geomagnetic storms but could not confirm any statistically significant storm-related changes [28]. Goncharenko et al. (2004) observed the storm-time increase in the neutral wind to altitudes as low as 100 km [29]. Pancheva et al. (2007) examined the short-term response of the MLT region using neutral wind data at northern high latitudes and found that the semidiurnal tide showed a very different response to the first and to the next two storms, with an enhancement and a reduction [30]. Yi et al. (2021) reported a significant increase in semidiurnal amplitudes in both zonal and meridional components during geomagnetic active periods in the MLT region at Davis Station, Antarctica [31]. Amplitudes of diurnal and semidiurnal tides were also found to be stronger at the solar minimum than at the solar maximum [32]. Under the influence of geomagnetic activities, the amplitude variations of semidiurnal and diurnal tides may also be affected by the season [33]. Furthermore, the enhancements of other oscillations with periods from hours to days can also be observed during geomagnetic storms, but those waves are rarely reported [34,35].

Insights into the physical process of how geomagnetic storms affect the ionosphere and the MLT region have also been investigated in previous studies. Fesen et al. (1993) found that the largest source of the semidiurnal meridional winds was the solar tides, while the semidiurnal zonal winds and temperatures were driven by solar forcing, auroral forcing, and vertically propagating waves from the lower atmosphere. The semidiurnal wind amplitudes generated by the auroral source increase strongly with increasing activity [36]. Fuller-Rowell (1995) suggested that advection might also play a role in transporting wind disturbances from high to lower latitudes in the lower thermosphere [37]. Nozawa and Brekke (1995) demonstrated that ion drag could partially explain the neutral wind disturbances in the E region [38]. Pancheva et al. (2003) found that the amplitude of the semidiurnal tide is not related to solar activity but mainly to its own variability [39]. According to Kutiev et al. (2007), from low to middle latitudes, the enhancement of semidiurnal tides may be related to enhancements of TEC in equatorial origins (ETEs) [40]. Pancheva et al. (2007) identified two main factors contributing to changes in neutral wind tides in the MLT region during geomagnetic storms. First, they noted an additional ionization in the MLT region caused by geomagnetic disturbances. Second, they observed that increased proton flux during solar proton events (SPE) could lead to ozone reductions, which results in temperature decreases and subsequently alters the pattern of neutral winds [32]. Moreover, particle precipitation and local electron density increase may also be a contributing factor [27,41]. Some studies have also suggested that the storm-time wind patterns are primarily controlled by pressure gradients associated with the high-latitude Joule heating, Coriolis force, and ion drag (or ion-neutral coupling) [30,42,43].

Currently, there are still issues in the literature on the changes of wave components in the atmosphere during geomagnetic storms, such as the unclear statistical conclusions, insufficient observations, and the detailed physical mechanisms of the geomagnetic storm's effects on the ionosphere and MLT variations. It subsequently affects the interpretation and exploration of the physical processes in the ionosphere and MLT during geomagnetic storms. In the present study, we propose to analyze the vertical TEC data and meteor

neutral wind data observed in Mohe (53.5°N, 122.3°E) and Beijing (40.3°N, 116.2°E) to investigate tidal variations during some intense geomagnetic storms.

2. Data and Methods

In this study, neutral wind data from meteor radars and vertical TEC data from the Global Navigation Satellite System at Mohe and Beijing, China, during 2016–2022 were obtained from the data center of the Chinese Meridian Project (https://dcstatus.meridianproject.ac.cn/) (accessed on 1 October 2024). Neutral wind data were available from 70 to 110 km with a 1 h temporal resolution and a 2 km height resolution. The TEC data were obtained from five satellites (C01–C05) of the BeiDou Navigation Satellite System with a time resolution of 30 s.

Geomagnetic data from the OMNI dataset (https://omniweb.gsfc.nasa.gov/) (accessed on 1 October 2024) were also used for analysis. Conventionally, a geomagnetic storm can be evaluated by the 1-h time resolution disturbance storm time (Dst) index or the 3-h Kp index. We diagnosed interplanetary conditions for each geomagnetic storm using the criteria of the Dst minimum value in a whole geomagnetic storm process. Intense geomagnetic storms with Dst minima of less than −100 nT were the focus of this study [44]. As shown in Table 1, there were six intense geomagnetic storms during 2016–2022. The maximum values of the Kp index during six storms are also listed in Table 1 [45,46].

Table 1. Overview of the six intense geomagnetic storms during 2016–2021.

Case Number	Storm Date	Kp Maximum	Dst Minimum (nT)	Category *
a	20 January 2016	6	−101	Intense
b	13 October 2016	6	−110	Intense
c	27 May 2017	7	−125	Intense
d	7 September 2017	8	−122	Intense
e	25 August 2018	7	−175	Intense
f	4 November 2021	8	−105	Intense

* Classification standard was based on the Dst minimum value [44,47].

In a sliding window with a length of 2 days and a step of 1 h, the neutral wind data are fitted by the least squares fitting method to estimate the tidal amplitudes and phases with the equation as follows [48]:

$$data_i = DC_i + \sum_{n=1}^{4} \left(a_{in} \cos \frac{2\pi t}{T_n} + b_{in} \sin \frac{2\pi t}{T_n} \right) \quad (1)$$

where $data_i$ corresponds to the neutral wind data and DC_i represents the background mean level. Different n stand for different fitting components (the diurnal tide, semidiurnal tide, 8-h tide, and 6-h tide) and $T_n = 24/n$ represents the period of the corresponding fitting component. Fitting results are marked at the end date of each window. Note that the tidal amplitudes are only derived when the available data are higher than 70% in each window. The same data processing methods were adopted for TEC data to estimate the amplitudes of tidal components in the ionosphere. Tidal amplitudes were averaged from all available data captured by five satellites from C01 to C05. The results of the 8-h and 6-h tides are not discussed in this study due to their weak amplitudes compared with the diurnal and semidiurnal tides.

3. Results

3.1. Tidal Variations in TEC during Geomagnetic Storms

Figure 1 presents the variations of diurnal tides in the ionospheric TEC at Mohe (blue lines) and Beijing (red lines) during six intense storms from 2016 to 2021. Two black dashed

lines in each subplot indicate the start and end times of the geomagnetic storms [49,50]. Amplitudes are not given at low data percentages or data gaps. As shown in Figure 1, the diurnal tides usually have an increase after the storm occurrence, except for a decrease in October 2016 (Figure 1b). The largest increase can be found in May 2017 (Figure 1c), with an enhancement of 4 TECU in the diurnal amplitudes at Beijing. The amplitudes of diurnal tides in Beijing are generally 2 TECU greater than those in Mohe, except for in November 2021 (Figure 1f).

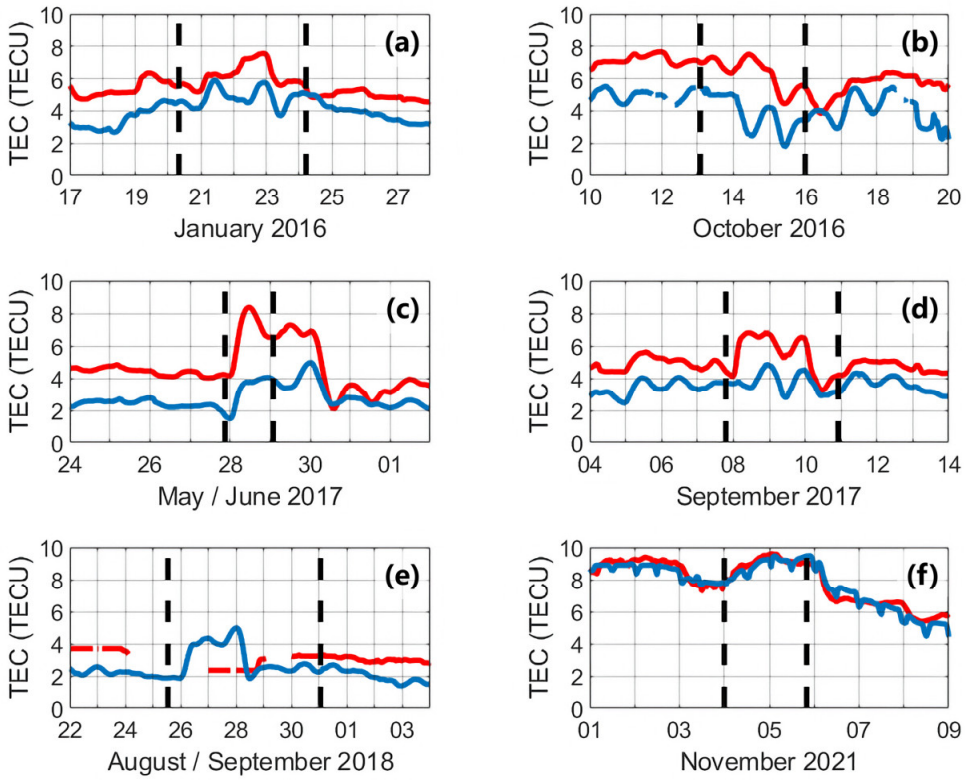

Figure 1. Amplitudes of diurnal tides in ionospheric TEC at Mohe (blue lines) and Beijing (red lines) during geomagnetic storms on: (**a**) 20 January 2016; (**b**) 13 October 2016; (**c**) 27 May 2017; (**d**) 7 September 2017; (**e**) 25 August 2018; and (**f**) 4 November 2021, respectively. The time ranges are from 3 days before the start time to 3 days after the end time of the six storms (indicated by two black dashed lines).

Figure 2 denotes the variations of semidiurnal tides in the ionospheric TEC of Mohe (blue lines) and Beijing (red lines) during six intense storms from 2016 to 2021. As shown in Figure 2, semidiurnal tidal amplitudes also reveal similar trends as the diurnal tides during storms. Enhancements are also obvious in two cases in 2017 (Figure 2c,d). However, the amplitudes of semidiurnal tides are usually comparable between Mohe and Beijing. Tsidu et al. (2014) observed the abrupt TEC changes in tidal amplitudes under the effects of a geomagnetic storm within the 20°S–20°N latitude band in January 2012; the diurnal amplitudes increased up to 5 TECU (about 83%, modulated by the storms) and semidiurnal amplitudes increased up to 2 TECU (about 30%) [22]. Nevertheless, from our statistical results shown in Figures 1 and 2, the occurrences of the enhancement of diurnal and semidiurnal tides at Mohe and Beijing varied in different cases. In order to present a clear comparison, Table 2 shows the maximum differences between the ionospheric enhanced tidal amplitudes and the seasonal average amplitudes. The results were checked from the onset to 3 days after the end of the geomagnetic storm.

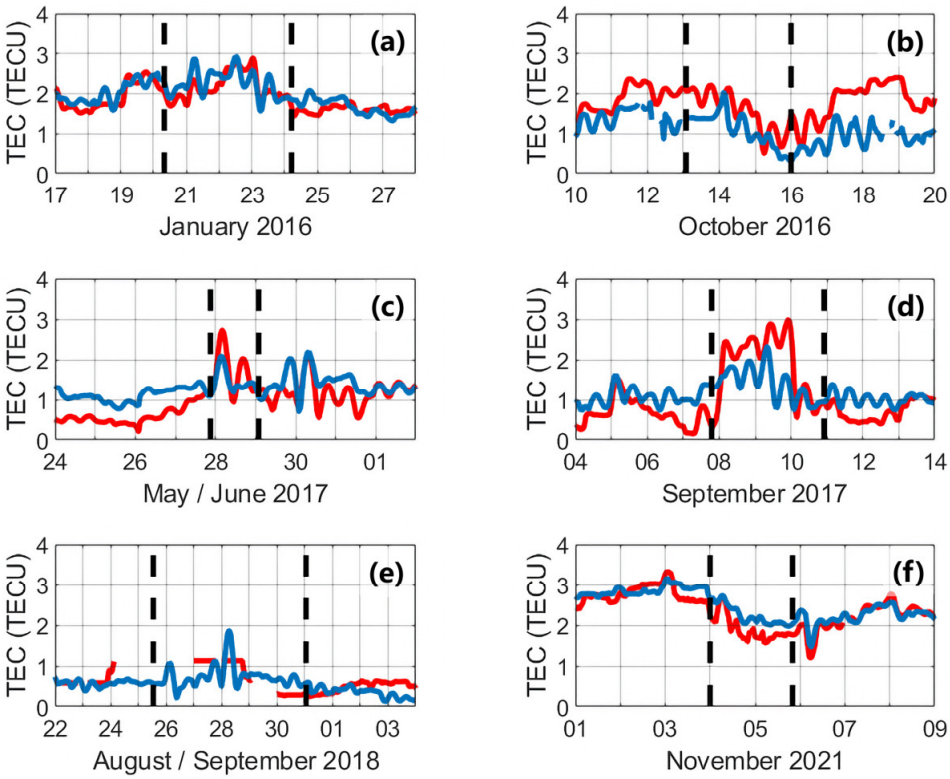

Figure 2. Same as Figure 1 but for semidiurnal tides during geomagnetic storms on: (**a**) 20 January 2016; (**b**) 13 October 2016; (**c**) 27 May 2017; (**d**) 7 September 2017; (**e**) 25 August 2018; and (**f**) 4 November 2021, respectively.

Table 2. The maximum difference in TEC between ionospheric tidal amplitudes during storms and seasonal average tidal amplitudes at Mohe and Beijing.

Case Number	Storm Date	Mohe		Beijing	
		Diurnal Tide	Semidiurnal Tide	Diurnal Tide	Semidiurnal Tide
a	20 January 2016	+0.5 TECU	+1.2 TECU	+0.1 TECU	+0.8 TECU
b	13 October 2016	+2.3 TECU	+0.5 TECU	+3.3 TECU	+0.8 TECU
c	27 May 2017	+2.2 TECU	+1.2 TECU	+3.8 TECU	+1.7 TECU
d	7 September 2017	+2.3 TECU	+1.3 TECU	+2.8 TECU	+2.1 TECU
e	25 August 2018	+2.9 TECU	+1.0 TECU	*	*
f	4 November 2021	+5.9 TECU	+0.9 TECU	+4.8 TECU	+1.0 TECU

* Results could not be determined due to missing data.

3.2. Tidal Variations in MLT Winds During Geomagnetic Storms

3.2.1. Diurnal Tides

Figures 3 and 4 present the amplitudes of diurnal tides in meridional and zonal winds in the MLT region at Mohe during six geomagnetic storms. The results are shown in an altitude range of 84–96 km to avoid uncertainties caused by missing data. Two black dashed lines in each subplot indicate the start and end times of the geomagnetic storms. White areas indicate low data percentages or data gaps. The diurnal amplitudes at Mohe are generally lower than 10 m/s. During geomagnetic storms, the variations of diurnal tidal amplitudes are not uniform and do not show significant responses to the occurrence of storms. Note that the amplitudes of diurnal tides also have some periodic variations (e.g., Figure 3e), which are due to other waves with periods around 24 h.

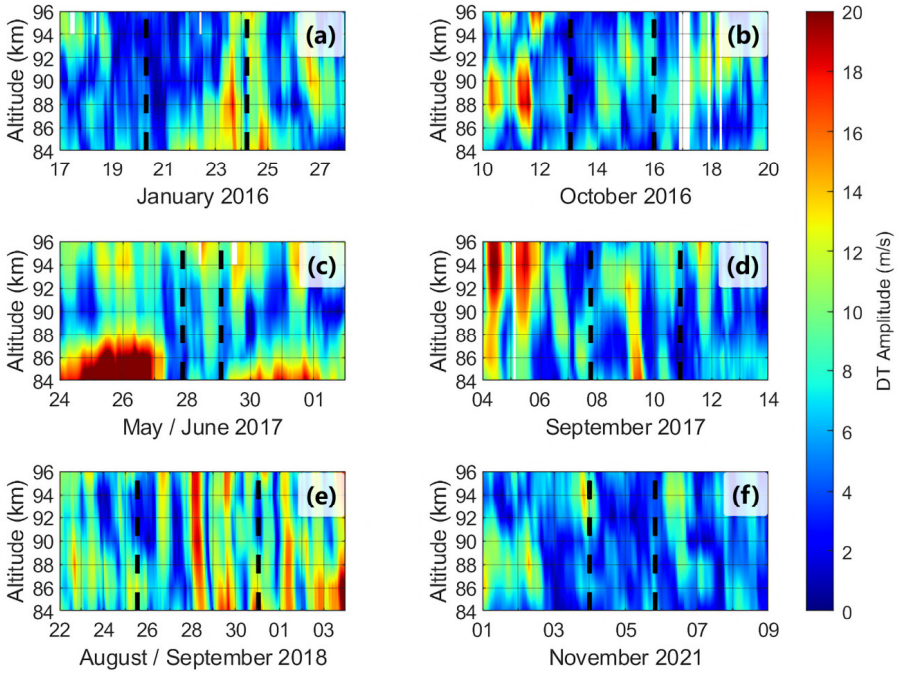

Figure 3. Amplitudes of MLT diurnal tides in the meridional component during geomagnetic storms at Mohe on: (**a**) 20 January 2016; (**b**) 13 October 2016; (**c**) 27 May 2017; (**d**) 7 September 2017; (**e**) 25 August 2018; and (**f**) 4 November 2021, respectively. The two black dashed lines represent the beginning and end of the geomagnetic storm.

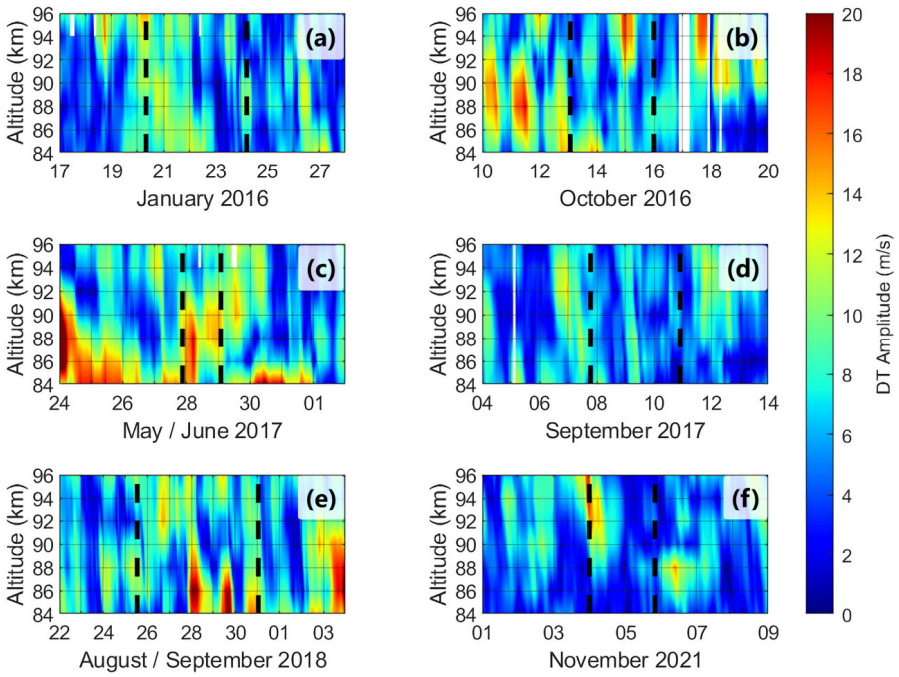

Figure 4. Same as Figure 3 but for diurnal tides in the zonal component at Mohe during geomagnetic storms on: (**a**) 20 January 2016; (**b**) 13 October 2016; (**c**) 27 May 2017; (**d**) 7 September 2017; (**e**) 25 August 2018; and (**f**) 4 November 2021, respectively.

Figures 5 and 6 present the variations of diurnal tides in meridional and zonal winds in the MLT region in Beijing during the six geomagnetic storms. The diurnal amplitudes in Beijing are generally around 20 m/s. It seems that the diurnal amplitudes notably increase during storms, especially in the zonal component. As shown in Figure 6, the largest amplitude reaches over 40 m/s (Figure 6a,d,f). However, diurnal amplitudes are

not enhanced in the zonal winds during the storm in May 2017 (Figure 6c). Compared with diurnal variations in Mohe, the diurnal amplitudes in Beijing are larger, with more evidenced enhancements during geomagnetic storms. Additionally, the variations of diurnal tides in meridional and zonal components are not consistent in most cases. In order to present a clear comparison, Table 3 shows the maximum differences between the MLT diurnal amplitudes and the seasonal average amplitudes.

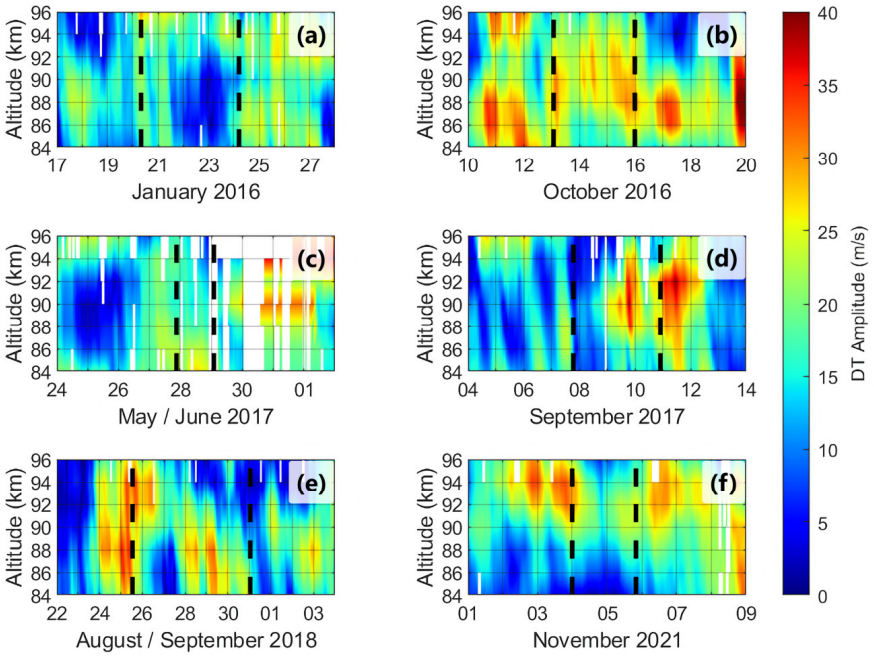

Figure 5. Same as Figure 3 but for diurnal tides in the meridional component at Beijing during geomagnetic storms on: (**a**) 20 January 2016; (**b**) 13 October 2016; (**c**) 27 May 2017; (**d**) 7 September 2017; (**e**) 25 August 2018; and (**f**) 4 November 2021, respectively.

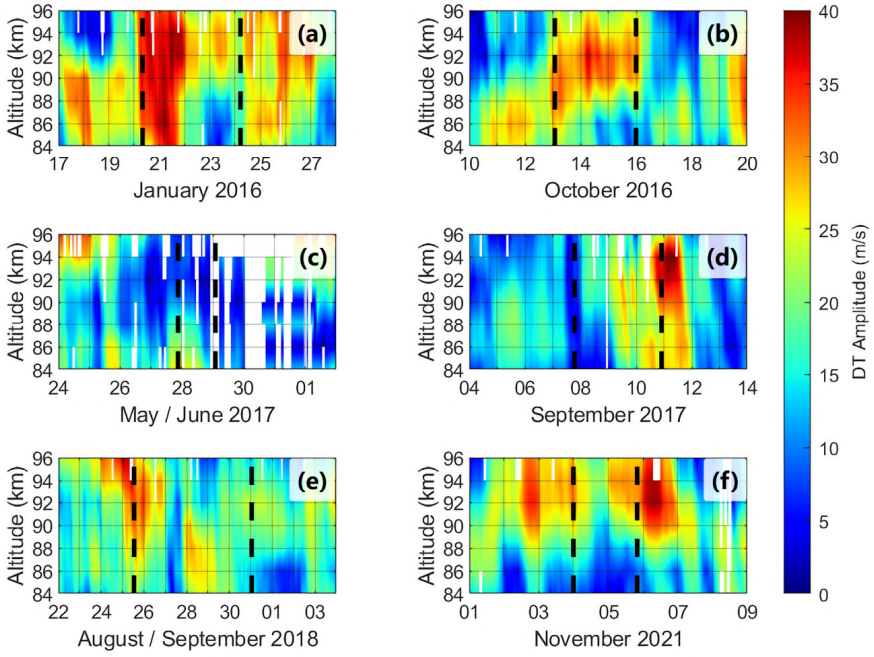

Figure 6. Same as Figure 3 but for diurnal tides in the zonal component at Beijing during geomagnetic storms on: (**a**) 20 January 2016; (**b**) 13 October 2016; (**c**) 27 May 2017; (**d**) 7 September 2017; (**e**) 25 August 2018; and (**f**) 4 November 2021, respectively.

Table 3. The maximum difference in winds between MLT diurnal amplitudes during storms and seasonal average tidal amplitudes at Mohe and Beijing.

Case number	Storm Date	Mohe (Diurnal Tide)		Beijing (Diurnal Tide)	
		Meridional	Zonal	Meridional	Zonal
a	20 January 2016	+11.6 m/s	+6.1 m/s	+9.9 m/s	+24.0 m/s
b	13 October 2016	+6.8 m/s	+8.3 m/s	+26.2 m/s	+26.3 m/s
c	27 May 2017	+8.3 m/s	+9.6 m/s	+22.8 m/s	*
d	7 September 2017	+8.1 m/s	+4.5 m/s	+23.0 m/s	+26.2 m/s
e	25 August 2018	+14.4 m/s	+12.5 m/s	+15.9 m/s	+15.1 m/s
f	4 November 2021	+5.2 m/s	+9.8 m/s	+19.2 m/s	+28.1 m/s

* Results could not be determined due to missing data.

3.2.2. Semidiurnal Tides

The variations of semidiurnal tides in meridional and zonal winds at Mohe during six geomagnetic storms are presented in Figures 7 and 8. Amplitudes of the semidiurnal tidal components are typically larger than the diurnal tides during the six geomagnetic storms. It seems that the amplitudes of the semidiurnal tides remarkably increase before or after the onset of the storms. The amplitudes reached 60 m/s during January 2016 and September 2017 (Figures 7a,d and 8a,d). In addition, January 2016 had the longest and strongest semidiurnal tides at Mohe among the six cases.

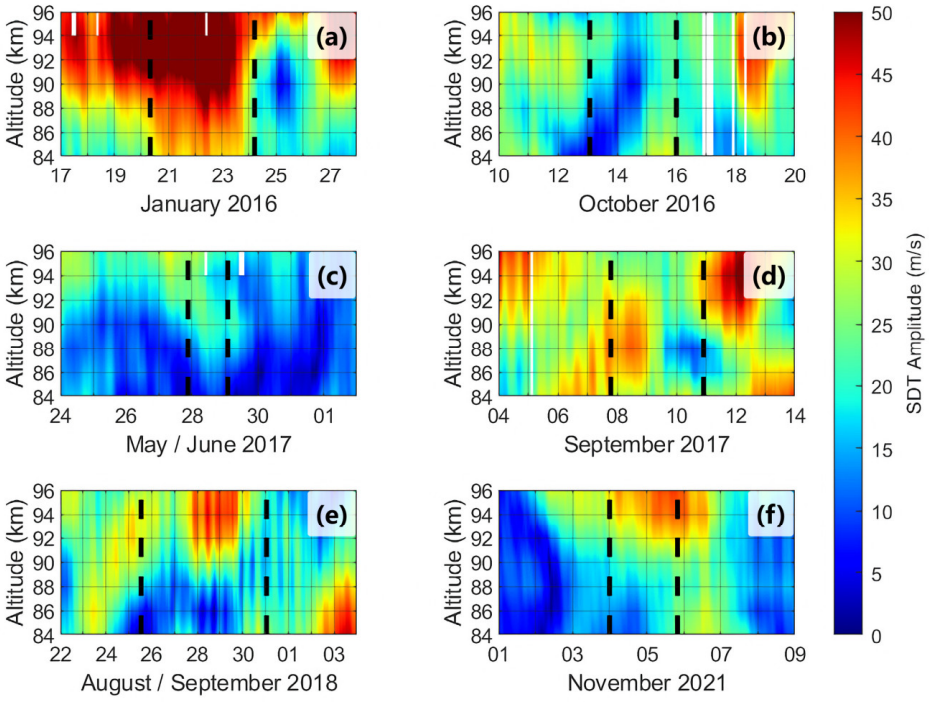

Figure 7. Same as Figure 3 but for semidiurnal tides in the meridional component at Mohe during geomagnetic storms on: (**a**) 20 January 2016; (**b**) 13 October 2016; (**c**) 27 May 2017; (**d**) 7 September 2017; (**e**) 25 August 2018; and (**f**) 4 November 2021, respectively.

The variations of semidiurnal tides during six geomagnetic storms at Beijing are presented in Figures 9 and 10. In order to present a clear comparison, Table 4 shows the maximum differences between the MLT semidiurnal amplitudes and the seasonal average amplitudes. Enhancements of semidiurnal tides can be observed during storms; for instance, in October 2016, September 2017, and November 2021 (Figures 9a,d,f and 10a,d,f). The largest amplitude reached 65 m/s in September 2017 (Figures 9d and 10d). Note that

the variations of semidiurnal tides in the meridional and zonal components are generally consistent during geomagnetic storms.

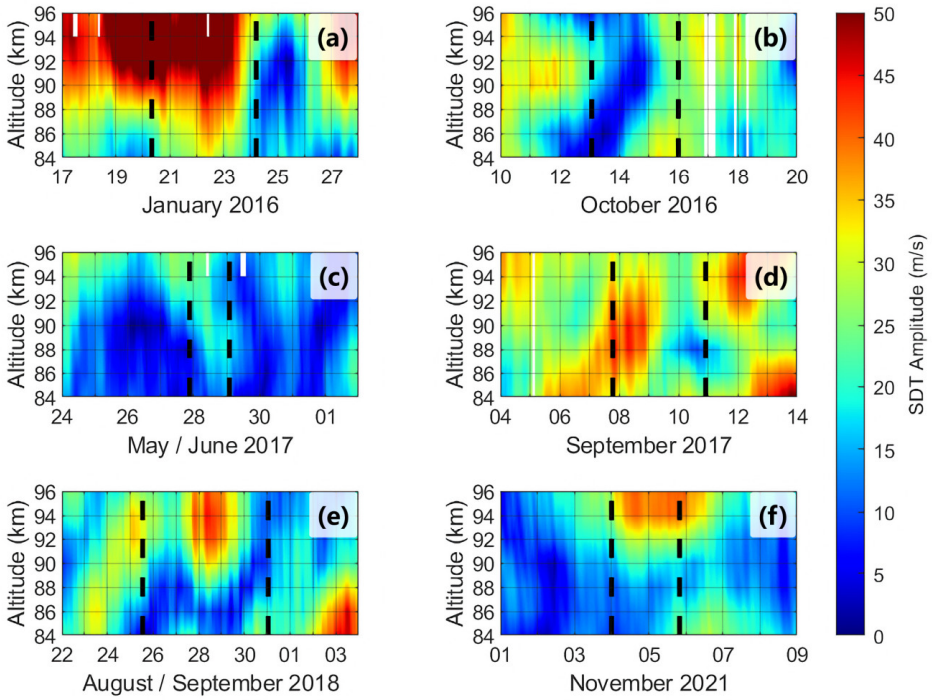

Figure 8. Same as Figure 3 but for semidiurnal tides in the zonal component at Mohe during geomagnetic storms on: (**a**) 20 January 2016; (**b**) 13 October 2016; (**c**) 27 May 2017; (**d**) 7 September 2017; (**e**) 25 August 2018; and (**f**) 4 November 2021, respectively.

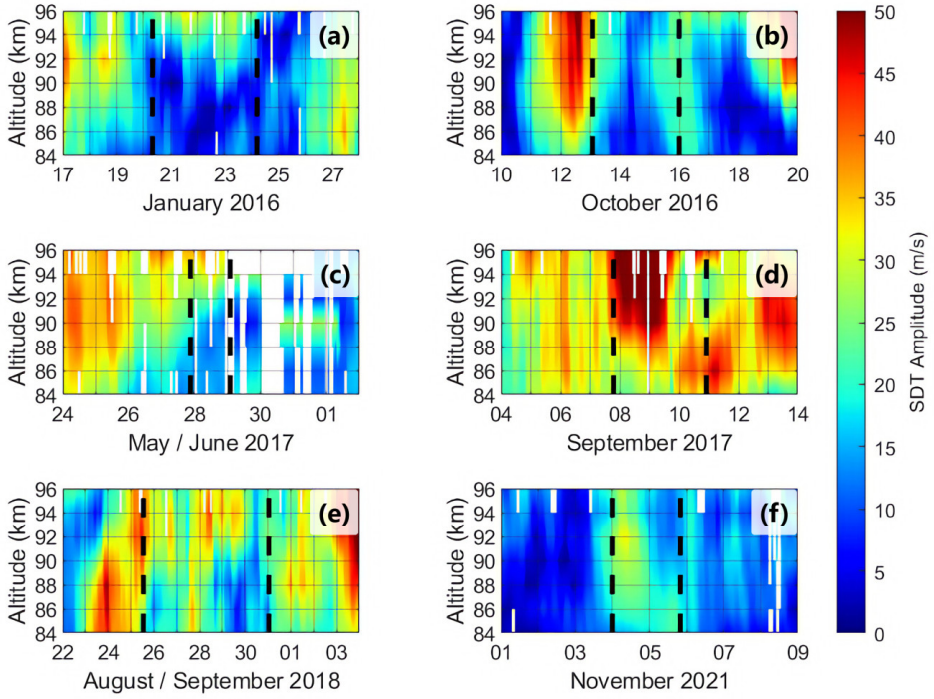

Figure 9. Same as Figure 3 but for semidiurnal tides in the meridional component at Beijing during geomagnetic storms on: (**a**) 20 January 2016; (**b**) 13 October 2016; (**c**) 27 May 2017; (**d**) 7 September 2017; (**e**) 25 August 2018; and (**f**) 4 November 2021, respectively.

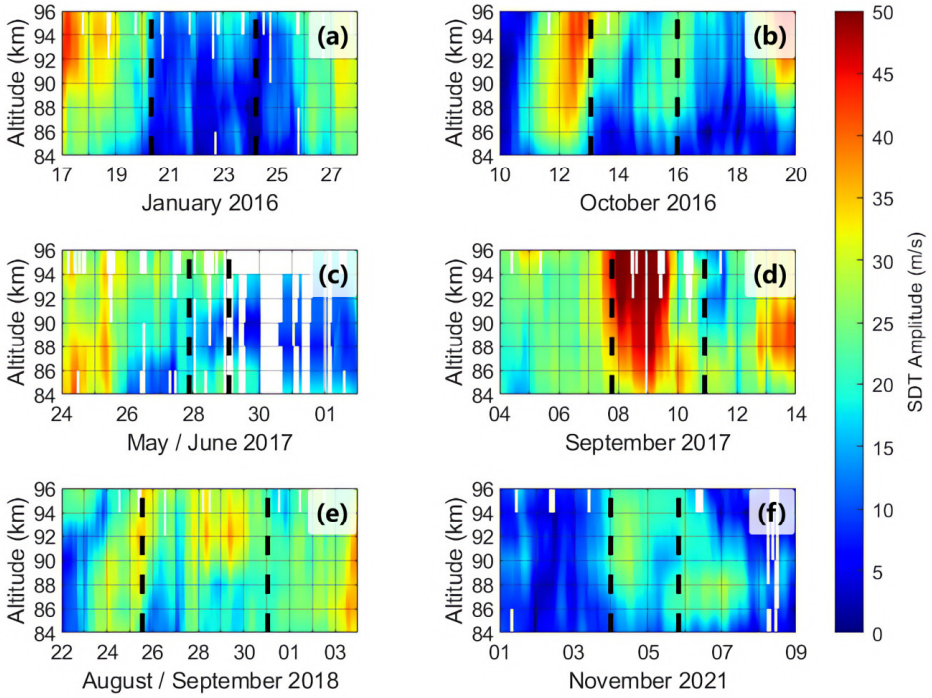

Figure 10. Same as Figure 3 but for semidiurnal tides in the zonal component at Beijing during geomagnetic storms on: (**a**) 20 January 2016; (**b**) 13 October 2016; (**c**) 27 May 2017; (**d**) 7 September 2017; (**e**) 25 August 2018; and (**f**) 4 November 2021, respectively.

Table 4. The maximum difference in winds between MLT semidiurnal amplitudes during storms and seasonal average tidal amplitudes at Mohe and Beijing.

Case Number	Storm Date	Mohe (Semidiurnal Tide)		Beijing (Semidiurnal Tide)	
		Meridional	Zonal	Meridional	Zonal
a	20 January 2016	+39.9 m/s	+33.1 m/s	+22.6 m/s	+17.8 m/s
b	13 October 2016	+14.3 m/s	+10.6 m/s	+27.2 m/s	+22.3 m/s
c	27 May 2017	+8.7 m/s	+10.0 m/s	*	*
d	7 September 2017	+29.2 m/s	+32.2 m/s	+39.7 m/s	+35.6 m/s
e	25 August 2018	+28.3 m/s	+29.6 m/s	+23.5 m/s	+18.3 m/s
f	4 November 2021	+14.1 m/s	+11.7 m/s	+11.3 m/s	+13.8 m/s

* Results could not be determined due to missing data.

Our observations indicate that responses of diurnal tides to storms are not obvious in the MLT region at Mohe and Beijing, but semidiurnal tides usually enhance during storms. Variations of diurnal tides are not consistent between meridional and zonal components, but the evolutions of semidiurnal tides are consistent in two components. Although semidiurnal tides usually increase in the MLT region during geomagnetic storms, the occurrences of enhanced semidiurnal tides are not uniform. Sometimes the enhancements are at the beginning of the geomagnetic storms, and sometimes they are observed at the end of the storms. Latitudinal variations are also found between Mohe and Beijing; tidal amplitudes often have different patterns at different latitudes during the same case.

4. Discussion

To further understand the effect of geomagnetic storms, we analyzed the seasonal variations of the tidal waves based on the long-term neutral wind data and TEC data. As discussed in Section 3, diurnal and semidiurnal tides present substantial variations during geomagnetic storms. However, they also have their own seasonal variations. To quantitatively analyze the effects of the geomagnetic storms, the enhanced amplitudes of

the semidiurnal tide (SDT) and the diurnal tide (DT) exceeding the seasonal level (more than two times the standard deviations from the seasonal mean) were speculated to be a result of the effects of geomagnetic storms. Since solar activity can affect the amplitudes of tidal waves, the seasonal mean was only derived in the same year of the storms. Excluding the period of the storms, the daily tidal amplitudes in the same season were used to calculate the seasonal mean and standard deviations. This examination also excluded the traditional tidal variations from lower altitudes. Nevertheless, it was difficult to determine the causality of the enhanced tidal waves in the ionospheric TEC and in the MLT wind data. If the effect of a geomagnetic storm on the tidal variation is strong enough, the amplitudes of SDTs/DTs in both TEC and MLT wind should be significantly larger than the climatological level during geomagnetic storms.

Tables 5 and 6 present whether or not (Y/N) the enhanced tidal amplitudes at Mohe and Beijing significantly exceeded the seasonal level during the six intense geomagnetic storms from 2016 to 2021. The results were checked from the onset to 3 days after the end of the geomagnetic storm. For tidal observations in the ionospheric TEC, diurnal tides were usually enhanced during storms at Mohe and Beijing, except for (a) in January 2016. Semidiurnal tides were not significantly enhanced in two cases in 2016, but exceeded the seasonal level during cases in 2017 and 2018.

Table 5. Whether or not (Y/N) the enhanced tidal amplitudes at Mohe significantly exceeded the seasonal level during six intense geomagnetic storms from 2016 to 2021. M and Z represent the meridional and zonal components, respectively.

Tides	Case (a)	Case (b)	Case (c)	Case (d)	Case (e)	Case (f)
Diurnal Tide (TEC)	N	Y	Y	Y	Y	Y
Diurnal Tide (M)	Y	N	N	N	Y	N
Diurnal Tide (Z)	N	Y	N	N	Y	Y
Semidiurnal Tide (TEC)	N	N	Y	Y	Y	N
Semidiurnal Tide (M)	Y	N	N	Y	Y	N
Semidiurnal Tide (Z)	Y	N	N	Y	Y	N

Table 6. Whether or not (Y/N) the enhanced tidal amplitudes at Beijing significantly exceeded the seasonal level during six intense geomagnetic storms from 2016 to 2021. M and Z represent the meridional and zonal components, respectively.

Tides	Case (a)	Case (b)	Case (c)	Case (d)	Case (e)	Case (f)
Diurnal Tide (TEC)	N	Y	Y	Y	*	Y
Diurnal Tide (M)	N	Y	Y	Y	Y	Y
Diurnal Tide (Z)	Y	Y	*	Y	Y	Y
Semidiurnal Tide (TEC)	N	N	Y	Y	*	Y
Semidiurnal Tide (M)	Y	Y	*	Y	Y	N
Semidiurnal Tide (Z)	Y	Y	*	Y	Y	N

* Results could not be determined due to missing data.

For the tidal variations in the MLT region, some tidal amplitudes were not significantly enhanced during geomagnetic storms. In addition, diurnal tides in the MLT region at Mohe were sometimes only significantly enhanced in one direction but kept within the seasonal level in the other direction (cases (a), (b), and (f)). It is also evident that Beijing, with a lower latitude, exhibited a more obvious phenomenon of tidal enhancement in neutral winds during geomagnetic storms compared to Mohe. Responses of diurnal and semidiurnal tides were only significantly enhanced both in the MLT region and ionosphere during the 2018 case, which had the lowest Dst index. However, according to other cases, the amplitude changes might not be proportional to the value of the Dst indices.

According to previous studies, four storms in cases (b), (c), (d), and (f) that occurred on 13 October 2016, 27 May 2017, 7 September 2017, and 4 November 2021 were caused by Coronal Mass Ejection (CME), while the storm in case (a) that occurred on 20 January 2016 was triggered by the Corotating Interaction Region (CIR), and the storm in case (e) that occurred on 25 August 2018 was jointly caused by the CIR and weak CME [51–54]. It seems that the CIR storm does not strengthen the tidal amplitudes in ionospheric TEC but may affect the semidiurnal tides in the MLT region (case (a)). Nevertheless, this feature needs to be checked with additional observations.

Notably, significant enhancements of the semidiurnal tides in the MLT region were observed at Mohe and Beijing prior to the onset of geomagnetic storms in cases (a), (b), and (c), although the semidiurnal amplitudes during these three cases had a decrease feature as the storms started. It is very interesting to note this characteristic. If the enhancements prior to the onset of storms are caused by the storms, the tidal effect of the storm might be firstly acted in the MLT region and then upward to the ionosphere. Moreover, the reduction of semidiurnal tides during storms observed in the MLT region in previous studies might be due to an earlier enhanced semidiurnal amplitude. These speculations need to be investigated in the future with more observational cases.

5. Summary and Conclusions

During six intense geomagnetic storms that occurred from 2016 to 2021, tidal variations in the ionospheric TEC and in the MLT region neutral winds were analyzed at Mohe and Beijing. The conclusions can be summarized as follows:

1. Ionospheric diurnal and semidiurnal tides in TEC are usually enhanced during intense geomagnetic storms, while the responses of diurnal and semidiurnal tides in the MLT region at middle latitudes are not always captured.
2. The responses of the tidal amplitude changes are not proportional to the value of Dst indices.
3. Beijing, being at a lower latitude, has a more obvious tidal response to geomagnetic storms in the MLT region than at Mohe.
4. Semidiurnal tides in the MLT region can be enhanced prior to the onset of the geomagnetic storms, which leads to a decreasing trend in their amplitudes during geomagnetic storms. Further analysis is needed to study the mechanism of these earlier enhanced semidiurnal tides and reveal their relationships with storms.

Author Contributions: Conceptualization, Z.M.; methodology, Z.M. and J.M.; software, J.M. and J.B.; validation, Z.M., J.Y. and D.L.; formal analysis, J.M., J.Y. and D.L.; investigation, J.M. and Z.M.; resources, Z.M. and J.L.; data curation, J.M. and J.B.; writing—original draft preparation, J.M. and Z.M.; writing—review and editing, J.M. and Z.M.; supervision, Z.M.; funding acquisition, Z.M. and J.L. All authors have read and agreed to the published version of the manuscript.

Funding: This research was supported by the National Natural Science Foundation of China (42127805, 42104145, 12241101, and 42174192), the Specialized Research Fund for State Key Laboratories and the Fundamental Research Funds for the Central Universities (2042024fg0004).

Data Availability Statement: The authors acknowledge the Space Physics Data Facility at Goddard Space Flight Center (https://omniweb.gsfc.nasa.gov/) (accessed on 1 October 2024) for providing Dst data. The authors also gratefully acknowledge the Chinese Meridian Project (https://dcstatus.meridianproject.ac.cn/) (accessed on 1 October 2024) for providing neutral wind data and TEC data at Mohe and Beijing, China.

Acknowledgments: We acknowledge the use of the data from Chinese Meridian Project, and the support by the Specialized Research Fund for State Key Laboratories.

Conflicts of Interest: The authors declare no conflict of interest.

References

1. Tsagouri, I.; Belehaki, A.; Moraitis, G.; Mavromichalaki, H. Positive and Negative Ionospheric Disturbances at Middle Latitudes during Geomagnetic Storms. *Geophys. Res. Lett.* **2000**, *27*, 3579–3582. [CrossRef]
2. Lastovicka, J. Monitoring and Forecasting of Ionospheric Space Weather—Effects of Geomagnetic Storms. *J. Atmos. Sol. Terr. Phys.* **2002**, *64*, 697–705. [CrossRef]
3. Chukwuma, V. On Positive and Negative Ionospheric Storms. *Acta Geod. Geophys. Hung.* **2007**, *42*, 1–21. [CrossRef]
4. Balan, N.; Alleyne, H.; Otsuka, Y.; Lekshmi, D.V.; Fejer, B.G.; McCrea, I. Relative Effects of Electric Field and Neutral Wind on Positive Ionospheric Storms. *Earth Planets Space* **2009**, *61*, 439–445. [CrossRef]
5. Pedatella, N.M.; Lei, J.; Larson, K.M.; Forbes, J.M. Observations of the Ionospheric Response to the 15 December 2006 Geomagnetic Storm: Long-duration Positive Storm Effect. *J. Geophys. Res.* **2009**, *114*, 2009JA014568. [CrossRef]
6. Yamamoto, A.; Ohta, Y.; Okuzawa, T.; Taguchi, S.; Tomizawa, I.; Shibata, T. Characteristics of TEC Variations Observed at Chofu for Geomagnetic Storms. *Earth Planet. Sp.* **2014**, *52*, 1073–1076. [CrossRef]
7. Wen, D.; Mei, D. Ionospheric TEC Disturbances over China during the Strong Geomagnetic Storm in September 2017. *Adv. Space Res.* **2020**, *65*, 2529–2539. [CrossRef]
8. Bojilova, R.; Mukhtarov, P. Comparative Analysis of Global and Regional Ionospheric Responses during Two Geomagnetic Storms on 3 and 4 February 2022. *Remote Sens.* **2023**, *15*, 1739. [CrossRef]
9. Sori, T.; Shinbori, A.; Otsuka, Y.; Tsugawa, T.; Nishioka, M. Characteristics of GNSS Total Electron Content Enhancements Over the Midlatitudes During a Geomagnetic Storm on 7 and 8 November 2004. *JGR Space Phys.* **2019**, *124*, 10376–10394. [CrossRef]
10. Gong, Y.; Zhou, Q. Incoherent Scatter Radar Study of the Terdiurnal Tide in the E- and F-region Heights at Arecibo. *Geophys. Res. Lett.* **2011**, *38*, 2011GL048318. [CrossRef]
11. Yu, T.; Wang, W.; Ren, Z.; Cai, X.; Liu, L.; He, M.; Pedatella, N.; Zhai, C. Diagnostic Analysis of the Physical Processes Underlying the Long-Duration O/N_2 Depletion During the Recovery Phase of the 8 June 2019 Geomagnetic Storm. *JGR Space Phys.* **2022**, *127*, e2022JA031075. [CrossRef]
12. Gong, Y.; Zhou, Q.; Zhang, S.; Aponte, N.; Sulzer, M.; Gonzalez, S. Midnight Ionosphere Collapse at Arecibo and Its Relationship to the Neutral Wind, Electric Field, and Ambipolar Diffusion. *J. Geophys. Res.* **2012**, *117*, 2012JA017530. [CrossRef]
13. Gong, Y.; Zhou, Q.; Zhang, S. A Study on Electric Field Mapping from the F Region to the E Region at Arecibo. *JGR Space Phys.* **2016**, *121*, 713–718. [CrossRef]
14. Gan, Q.; Eastes, R.W.; Wu, Y.; Qian, L.; Cai, X.; Wang, W.; England, S.L.; McClintock, W.E. Thermospheric Responses to the 3 and 4 November 2021 Geomagnetic Storm During the Main and Recovery Phases as Observed by NASA's GOLD and ICON Missions. *Geophys. Res. Lett.* **2024**, *51*, e2023GL106529. [CrossRef]
15. Gong, Y.; Zhou, Q.; Zhang, S.; Aponte, N.; Sulzer, M. An Incoherent Scatter Radar Study of the Midnight Temperature Maximum That Occurred at Arecibo during a Sudden Stratospheric Warming Event in January 2010. *JGR Space Phys.* **2016**, *121*, 5571–5578. [CrossRef]
16. Gong, Y.; Zhou, Q.; Zhang, S. Atmospheric Tides in the Low-latitude E and F Regions and Their Responses to a Sudden Stratospheric Warming Event in January 2010. *JGR Space Phys.* **2013**, *118*, 7913–7927. [CrossRef]
17. Gong, Y.; Zhou, Q.; Zhang, S.D.; Aponte, N.; Sulzer, M.; González, S.A. The F Region and Topside Ionosphere Response to a Strong Geomagnetic Storm at Arecibo. *JGR Space Phys.* **2013**, *118*, 5177–5183. [CrossRef]
18. Li, J.; Wei, G.; Wang, W.; Luo, Q.; Lu, J.; Tian, Y.; Xiong, S.; Sun, M.; Shen, F.; Yuan, T.; et al. A Modeling Study on the Responses of the Mesosphere and Lower Thermosphere (MLT) Temperature to the Initial and Main Phases of Geomagnetic Storms at High Latitudes. *JGR Atmos.* **2023**, *128*, e2022JD038348. [CrossRef]
19. Li, J.; Wang, W.; Lu, J.; Yuan, T.; Yue, J.; Liu, X.; Zhang, K.; Burns, A.G.; Zhang, Y.; Li, Z. On the Responses of Mesosphere and Lower Thermosphere Temperatures to Geomagnetic Storms at Low and Middle Latitudes. *Geophys. Res. Lett.* **2018**, *45*, 128–137. [CrossRef]
20. Wang, W.; Lei, J.; Burns, A.G.; Solomon, S.C.; Wiltberger, M.; Xu, J.; Zhang, Y.; Paxton, L.; Coster, A. Ionospheric Response to the Initial Phase of Geomagnetic Storms: Common Features. *J. Geophys. Res.* **2010**, *115*, 2009JA014461. [CrossRef]
21. Li, J.; Wang, W.; Lu, J.; Yue, J.; Burns, A.G.; Yuan, T.; Chen, X.; Dong, W. A Modeling Study of the Responses of Mesosphere and Lower Thermosphere Winds to Geomagnetic Storms at Middle Latitudes. *JGR Space Phys.* **2019**, *124*, 3666–3680. [CrossRef]
22. Tsidu, G.M.; Abraha, G. Moderate Geomagnetic Storms of 22–25 January 2012 and Their Influences on the Wave Components in Ionosphere and Upper Stratosphere-Mesosphere Regions. *Adv. Space Res.* **2014**, *54*, 1793–1812. [CrossRef]

23. Pancheva, D.; Mukhtarov, P.; Andonov, B. Global Structure of Ionospheric TEC Anomalies Driven by Geomagnetic Storms. *J. Atmos. Sol. -Terr. Phys.* **2016**, *145*, 170–182. [CrossRef]
24. Wand, R.H. Geomagnetic Activity Effects on Semidiurnal Winds in the Lower Thermosphere. *J. Geophys. Res.* **1983**, *88*, 9243–9248. [CrossRef]
25. Manson, A.H.; Meek, C.E. The Effects of Geomagnetic Disturbances and Atmospheric Tides upon Middle Atmosphere Winds and MF Radar Scatter at Saskatoon (52°N, 107°W, 61° Geomagnetic). *J. Geophys. Res.* **1991**, *96*, 915–926. [CrossRef]
26. Singer, W.; Bremer, J.; Hoffmann, P.; Manson, A.H.; Meek, C.E.; Schminder, R.; Kürschner, D.; Portnyagin, Y.I.; Makarov, N.A.; Muller, H.G. Geomagnetic Influences upon Tides—Winds from MLT Radars. *J. Atmos. Terr. Phys.* **1994**, *56*, 1301–1311. [CrossRef]
27. Zhang, S.P.; Salah, J.E.; Mitchell, N.; Singer, W.; Murayama, Y.; Clark, R.R.; Van Eyken, A.; Thayer, J. Responses of the Mesospheric Wind at High Latitudes to the April 2002 Space Storm. *Geophys. Res. Lett.* **2003**, *30*, 2003GL018521. [CrossRef]
28. Balan, N.; Kawamura, S.; Nakamura, T.; Yamamoto, M.; Fukao, S.; Igarashi, K.; Maruyama, T.; Shiokawa, K.; Otsuka, Y.; Ogawa, T.; et al. Simultaneous Mesosphere/Lower Thermosphere and Thermospheric F Region Observations during Geomagnetic Storms. *JGR Space Phys.* **2004**, *109*, 2003JA009982. [CrossRef]
29. Goncharenko, L.P.; Salah, J.E.; Foster, J.C.; Huang, C. Variations in Lower Thermosphere Dynamics at Midlatitudes during Intense Geomagnetic Storms. *JGR Space Phys.* **2004**, *109*, 2003JA010244. [CrossRef]
30. Pancheva, D.; Singer, W.; Mukhtarov, P. Regional Response of the Mesosphere–Lower Thermosphere Dynamics over Scandinavia to Solar Proton Events and Geomagnetic Storms in Late October 2003. *J. Atmos. Sol. Terr. Phys.* **2007**, *69*, 1075–1094. [CrossRef]
31. Yi, W.; Reid, I.M.; Xue, X.; Murphy, D.J.; Vincent, R.A.; Zou, Z.; Chen, T.; Wang, G.; Dou, X. First Observations of Antarctic Mesospheric Tidal Wind Responses to Recurrent Geomagnetic Activity. *Geophys. Res. Lett.* **2021**, *48*, e2020GL089957. [CrossRef]
32. Andrioli, V.F.; Xu, J.; Batista, P.P.; Resende, L.C.A.; Da Silva, L.A.; Marchezi, J.P.; Li, H.; Wang, C.; Liu, Z.; Guharay, A. New Findings Relating Tidal Variability and Solar Activity in the Low Latitude MLT Region. *JGR Space Phys.* **2022**, *127*, e2021JA030239. [CrossRef]
33. Fahrutdinova, A.N.; Sherstyukov, O.N.; Maksyutin, S.V. Geomagnetic Activity Influence on the Dynamics of the Upper Mesosphere and Lower Thermosphere. *Int. J. Geomagn. Aeron.* **2001**, *2*, 201–208.
34. Li, Y.; Chen, G.; Zhang, S.; Huang, K.; Gong, W.; Zhang, M. Observational Evidence for the Neutral Wind Responses in the Mid-Latitude Lower Thermosphere to the Strong Geomagnetic Activity. *Space Weather* **2024**, *22*, e2023SW003830. [CrossRef]
35. Ma, Z.; Gong, Y.; Zhang, S.; Xue, J.; Luo, J.; Zhou, Q.; Huang, C.; Huang, K.; Yu, Y.; Li, G. Study of a Quasi-27-Day Wave in the MLT Region During Recurrent Geomagnetic Storms in Autumn 2018. *JGR Space Phys.* **2021**, *126*, e2020JA028865. [CrossRef]
36. Fesen, C.G.; Richmond, A.D.; Roble, R.G. Theoretical Effects of Geomagnetic Activity on Thermospheric Tides. *J. Geophys. Res.* **1993**, *98*, 15599–15612. [CrossRef]
37. Johnson, R.M.; Killeen, T.L. (Eds.) *The Upper Mesosphere and Lower Thermosphere: A Review of Experiment and Theory: Johnson/The Upper Mesosphere and Lower Thermosphere: A Review of Experiment and Theory*; Geophysical Monograph Series; American Geophysical Union: Washington, DC, USA, 1995; ISBN 978-1-118-66424-7.
38. Nozawa, S.; Brekke, A. Studies of the *E* Region Neutral Wind in the Disturbed Auroral Ionosphere. *J. Geophys. Res.* **1995**, *100*, 14717–14734. [CrossRef]
39. Pancheva, D.; Mitchell, N.; Middleton, H.; Muller, H. Variability of the Semidiurnal Tide Due to Fluctuations in Solar Activity and Total Ozone. *J. Atmos. Sol. Terr. Phys.* **2003**, *65*, 1–19. [CrossRef]
40. Kutiev, I.; Otsuka, Y.; Saito, A.; Tsugawa, T. Low-latitude Total Electron Content Enhancement at Low Geomagnetic Activity Observed over Japan. *J. Geophys. Res.* **2007**, *112*, 2007JA012385. [CrossRef]
41. Ma, G.; Igarashi, K.; Hocke, K. Mid-Latitude Winds in the Mesosphere: A Superposed Epoch Analysis over the Geomagnetic Storm Times. *J. Atmos. Sol. -Terr. Phys.* **2001**, *63*, 1993–2001. [CrossRef]
42. Emery, B.A.; Lathuillere, C.; Richards, P.G.; Roble, R.G.; Buonsanto, M.J.; Knipp, D.J.; Wilkinson, P.; Sipler, D.P.; Niciejewski, R. Time Dependent Thermospheric Neutral Response Tothe 2–11 November 1993 Storm Period. *J. Atmos. Sol. Terr. Phys.* **1999**, *61*, 329–350. [CrossRef]
43. Hagan, M.E.; Sipler, D.P. Combined Incoherent Scatter Radar and Fabry-Perot Interferometer Measurements of Frictional Heating Effects over Millstone Hill during March 7–10, 1989. *J. Geophys. Res.* **1991**, *96*, 289–296. [CrossRef]
44. Cander, L.R.; Mihajlovic, S.J. Forecasting Ionospheric Structure during the Great Geomagnetic Storms. *J. Geophys. Res.* **1998**, *103*, 391–398. [CrossRef]
45. Kutiev, I.; Tsagouri, I.; Perrone, L.; Pancheva, D.; Mukhtarov, P.; Mikhailov, A.; Lastovicka, J.; Jakowski, N.; Buresova, D.; Blanch, E. Solar Activity Impact on the Earth's Upper Atmosphere. *J. Space Weather Space Clim.* **2013**, *3*, A06. [CrossRef]
46. Koucká Knížová, P.; Laštovička, J.; Kouba, D.; Mošna, Z.; Podolská, K.; Potužníková, K.; Šindelářová, T.; Chum, J.; Rusz, J. Ionosphere Influenced from Lower-Lying Atmospheric Regions. *Front. Astron. Space Sci.* **2021**, *8*, 651445. [CrossRef]
47. Loewe, C.A.; Prölss, G.W. Classification and Mean Behavior of Magnetic Storms. *J. Geophys. Res.* **1997**, *102*, 14209–14213. [CrossRef]
48. Wu, D.L.; Hays, P.B.; Skinner, W.R. A Least Squares Method for Spectral Analysis of Space-Time Series. *J. Atmos. Sci.* **1995**, *52*, 3501–3511. [CrossRef]
49. Perreault, P.; Akasofu, S.I. A Study of Geomagnetic Storms. *Geophys. J. Int.* **1978**, *54*, 547–573. [CrossRef]
50. Yokoyama, N.; Kamide, Y. Statistical Nature of Geomagnetic Storms. *J. Geophys. Res.* **1997**, *102*, 14215–14222. [CrossRef]

51. Akala, A.O.; Oyeyemi, E.O.; Amaechi, P.O.; Radicella, S.M.; Nava, B.; Amory-Mazaudier, C. Longitudinal Responses of the Equatorial/Low-Latitude Ionosphere Over the Oceanic Regions to Geomagnetic Storms of May and September 2017. *JGR Space Phys.* **2020**, *125*, e2020JA027963. [CrossRef]
52. Arowolo, O.A.; Akala, A.O.; Oyeyemi, E.O. Interplanetary Origins of Some Intense Geomagnetic Storms During Solar Cycle 24 and the Responses of African Equatorial/Low-Latitude Ionosphere to Them. *JGR Space Phys.* **2021**, *126*, e2020JA027929. [CrossRef]
53. Lissa, D.; Venkatesh, K.; Prasad, D.; Niranjan, K. Distinct Ionospheric Response to Three Different Geomagnetic Storms during 2016 Using GPS-TEC Observations over the Indian Equatorial and Low Latitude Sectors. *Adv. Space Res.* **2022**, *70*, 1089–1103. [CrossRef]
54. Zhai, C.; Chen, Y.; Cheng, X.; Yin, X. Spatiotemporal Evolution and Drivers of the Four Ionospheric Storms over the American Sector during the August 2018 Geomagnetic Storm. *Atmosphere* **2023**, *14*, 335. [CrossRef]